PCCP

Origin of Hydroxyl Pair Formation on Reduced Anatase TiO2(101)

Journal:	*Physical Chemistry Chemical Physics*
Manuscript ID	CP-ART-03-2023-001051.R1
Article Type:	Paper
Date Submitted by the Author:	14-Apr-2023
Complete List of Authors:	Adamsen, Kræn; Aarhus Universitet Science and Technology, Interdisciplinary Nanoscience Center (iNANO) Petrik, Nikolay; Pacific Northwest National Laboratory, Physical and Computational Sciences Directorate Dononelli, Wilke; University of Bremen, d. MAPEX Center for Materials and Processes, Bremen Center for Computational Materials Science and Hybrid Materials Interfaces Group Kimmel, Greg; Pacific Northwest National Laboratory, Physical Sciences Division Xu, Tao; Aarhus University, Interdisciplinary Nanoscience Center (iNANO) Li, Zheshen; Aarhus University, Dept. of Physics and Astronomy Lammich, Lutz; Aarhus University, Department of Physics and Astronomy; Aarhus University, Interdisciplinary Nanoscience Center (iNANO) Hammer, Bjork; University of Aarhus, Physics and Astronomy Lauritsen, Jeppe; Aathus University, Interdisciplinary Nanoscience Center Wendt, Stefan; Aarhus University, Interdisciplinary Nanoscience Center (iNANO)

ARTICLE

Origin of hydroxyl pair formation on reduced anatase TiO_2(101)

Kræn C. Adamsen,[a] Nikolay G. Petrik,*[b] Wilke Dononelli,[c,d] Greg A. Kimmel,[b] Tao Xu,[a] Zheshen Li,[c] Lutz Lammich,[a,c] Bjørk Hammer,[c] Jeppe V. Lauritsen[a] and Stefan Wendt*[a]

Received 00th February 20xx,
Accepted 00th XXXX 20xx

DOI: 10.1039/x0xx00000x

The interaction of water with metal oxide surfaces is of key importance to several research fields and applications. Because of its ability to photo-catalyze water splitting, reducible anatase TiO_2 (a-TiO_2) is of particular interest. Here, we combine experiments and theory to study the dissociation of water on bulk-reduced a-TiO_2(101). Following large water exposures at room temperature, point-like protrusions appear on the a-TiO_2(101) surface, as shown by scanning tunneling microscopy (STM). These protrusions originate from hydroxyl pairs, consisting of terminal and bridging OH groups, OH_t / OH_b, as revealed by infrared reflection absorption spectroscopy (IRRAS) and valence band experiments. Utilizing density functional theory (DFT) calculations, we offer a comprehensive model of the water / a-TiO_2(101) interaction. This model also explains why the hydroxyl pairs are thermally stable up to ~480 K.

1 Introduction

Reducible metal oxides are of high interest in research fields such as photo-electrocatalysis, gas sensors, and heterogen-eous catalysis.[1-10] To advance these fields, good understanding of molecular interactions with reducible metal oxides is essential. Particularly the water / oxide interaction is important, because water is fundamental in several physical and chemical processes and it is almost everywhere.[11-13] Titania (TiO_2) is a very promising, prototypical reducible metal oxide,[6, 7, 9, 10 6, 7, 9, 10] and the interactions of numerous molecules with its surfaces have been studied.[7-9, 14-16]

A wealth of studies have addressed the thermodynamically stable rutile TiO_2(110) surface (r-TiO_2(110)),[7, 9, 14, 15, 17] and water / r-TiO_2(110) is one of the most intensely studied systems in oxide surface science.[9, 13-15, 18-28] On the one hand, it is known since long that water molecules dissociate at surface O vacancies (O_{vac}'s).[9, 15, 18-24] On the other hand, it has long been debated whether water also dissociates on stoichiometric surface areas, i.e. at regular 5-fold coordinated Ti sites (5f–Ti).[13, 27, 28]

Meanwhile, a number of studies appeared addressing also the technically very relevant anatase TiO_2(101) surface (a-TiO_2(101)).[16] Notice that the a-TiO_2(101) surface is the most stable and thus predominating facet of a-TiO_2 nanoparticles.[29] Owing to the ability of TiO_2 nanoparticles to photo-catalyze water splitting,[8-10] it is crucial to understand the water / a-TiO_2(101) interaction as a benchmark system. The a-TiO_2(101) surface is unreconstructed and has a sawtooth-like appearance, containing two under-coordinated sites: the 5f–Ti and the 2-fold coordinated O sites (2f–O), see Fig. 1a,b. After its preparation in ultrahigh vacuum (UHV) using standard recipes,[30, 31] there are no O_{vac}'s on the very surface. Instead, O_{vac}'s are located in the subsurface region of a-TiO_2(101).[32-34] This is in stark contrast to the r-TiO_2(110) surface, where plenty of O_{vac}'s are present on the very surface.[7, 9, 14, 15, 19]

Several research groups have studied the interaction of water with the a-TiO_2(101) surface.[33, 35-48] At low temperature (< 200 K) and at low coverages, water was found to adsorb molecularly on a-TiO_2(101).[33, 35, 36, 38, 45-47] By contrast, evidence for partly dissociated water was found following heating of water multilayers,[41-44] and at higher water pressures in room temperature (RT) experiments.[37, 40] Thus far, a link between these different experimental findings and an atomistic understanding is lacking. For example, there is a discrepancy between X-ray photoelectron spectroscopy (XPS) and STM studies. Whereas most XPS studies point toward mixed dissociative and molecular water adsorption,[37, 41-43] STM studies predominantly reported molecularly adsorbed water on a-TiO_2(101).[33, 36, 45, 46]

The adsorption of water on a-TiO_2(101) was also modeled using DFT calculations, see, for example, Refs. [33, 36, 49-54]. Most of these DFT calculations point to molecular adsorption on non-defected (stoichiometric) a-TiO_2(101) at low coverages. However, with the introduction of electron donors such as O_{vac}'s, Ti interstitials or impurities such as Nb dopants, water dissociation was found to be favorable.[33, 51, 53] Li and Gao's DFT calculations[51] promoted the idea that subsurface O_{vac}'s facilitate water dissociation on a-TiO_2(101). Taking all the experimental and theoretical studies together, the nature of water adsorption on a-TiO_2(101) is still puzzling. Whereas it is now clear that some water molecules indeed adsorb dissociatively, the mechanism for this process is elusive.

[a] Interdisciplinary Nanoscience Center (iNANO), Aarhus University, DK-8000 Aarhus C, Denmark, E-mail: swendt@inano.au.dk
[b] Physical Sciences Division, Pacific Northwest National Laboratory, Richland, Washington 99352, USA, E-mail: nikolay.petrik@gmail.com
[c] Department of Physics and Astronomy, Aarhus University, DK-8000 Aarhus C, Denmark
[d] MAPEX Center for Materials and Processes, Bremen Center for Computational Materials Science and Hybrid Materials Interfaces Group, Bremen University, 28359 Bremen, Germany.

†Electronic Supplementary Information (ESI) available: For ESI and additional DFT results see DOI: 10.1039/x0xx00000x

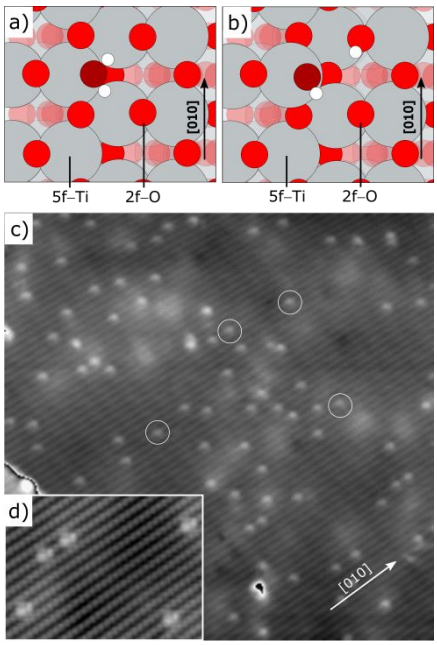

Fig. 1 Possible adsorption states of water on a-TiO_2(101) and STM measurements after high water exposures at RT. (a) Ball model of molecularly adsorbed water on a-TiO_2(101) (top view). The water molecule forms a dative bond to the under-coordinated 5f–Ti site. (b) Ball model of a OH_t / OH_b–pair adsorbed on a-TiO_2(101). OH_t groups adsorb on 5f–Ti sites and OH_b groups on neighboring 2f–O surface sites. Both structures result from DFT calculations that are described in the text. In a) and b), 5f–Ti and 2f–O sites are indicated. O atoms of the adsorbed water molecule and of OH_t are shown as dark red balls, and H's are shown as small white balls. (c) Large scale STM image (40 × 40 nm) of a-TiO_2(101) acquired after 60 L H_2O exposure at RT. Evenly distributed, bright features (white circles) are assigned to OH_t / OH_b–pairs. (d) High-resolution STM image (15 × 10 nm) of the same surface.

Here we utilized STM, XPS, temperature-programmed desorption (TPD), electron-stimulated desorption (ESD) and IRRAS experiments to study the effect of relatively large water exposures onto bulk-reduced a-TiO_2(101). We found the formation of paired hydroxyls groups upon water exposure at RT and after annealing of water multilayers. The hydroxyl pairs consist of neighboring terminal and bridging hydroxyls (OH_t / OH_b or OD_t / OD_b) and are stable up to ~480 K. The presented data and our proposed DFT-based reaction mechanism provide a deep understanding of the water interaction with reduced a-TiO_2(101) and reconcile previous studies.

2 Experimental section

Experimental details

The STM images were acquired in the constant current mode with a home-built Aarhus STM[55, 56] that was mounted in an UHV chamber with a base pressure of ~8 × 10^{-11} Torr. This UHV chamber was additionally equipped with a quadrupole mass spectrometer (Hiden Analytic), an AES instrument (Physical Electronics) an Ar ion source and capabilities for heating and cooling of the sample. For further details of this apparatus, see Ref. [57]. The STM measurements were conducted at RT using a Pt/Ir tip. STM images were acquired in Aarhus (Denmark) using tunneling voltages, V_S, of ~+1.0 V and tunneling currents, I_T, of ~0.1 nA.

The valence band (VB) XPS spectra were acquired at the ASTRID2 synchrotron source at ISA, Centre for storage ring facilities, Aarhus, at the AU-MatLine beamline.[58] This setup is equipped with a SX-700 monochromator, a SPECS Phoibos 150 electron energy analyzer and a similar setup for sample preparation as available in the STM chamber. The VB spectra were acquired using a photon energy of 170 eV.

The IRRAS, TPD and ESD experiments were performed in an UHV system with a base pressure of ~1 × 10^{-10} Torr that has been described previously.[48, 59] The system (at PNNL, Richland, USA) is equipped with a molecular beam source, a closed-cycle helium cryostat for sample cooling, a low-energy electron gun (Kimball Physics, Model ELG-2), a quadrupole mass spectrometer (Extrel, Model EXM 720), and a Fourier-transform infrared (FTIR) spectrometer (Bruker, Model Vertex 80) for IRRAS measurements performed in external reflection mode. In the IRRAS experiments, the p-polarized infrared (IR) light was incident on the a-TiO_2(101) single crystal at 20° to the [10$\bar{1}$] azimuth and grazing incidence (~85°, with respect to the surface normal) and detected in the specular direction. The resolution was set to 4 cm^{-1}. All IRRAS spectra were acquired at 30 K.

In both laboratories, natural a-TiO_2(101) single crystals (SurfaceNet) were prepared either by Ar^+ or Ne^+ sputtering and annealing in O_2 at 720–950 K and subsequent sputtering followed by vacuum-annealing, likewise at 820–950 K. Such preparation cycles (with and without O_2) were repeated until the surfaces were found clean (judged by STM and XPS, or TPD and LEED). In each case, the sample temperature was monitored by a K-type thermocouple spot-welded to the back of the sample plate. Water ($H_2{}^{16}O$, $H_2{}^{18}O$, D_2O) was cleaned via several freeze-pump-thaw cycles. In Aarhus, water was dosed via back-filling the UHV chambers through leak valves. At PNNL, a molecular beam was used to dose water. Water exposures are given either in monolayer (ML) equivalents (1 ML = density of 5f–Ti sites = 5.2 × 10^{14} molecules/cm^2) or in Langmuir (L; 1 L = 1 × 10^{-6} Torr × s). More experimental details are given in the ESI.

Computational details

Electronic structure calculations were performed using DFT with the plane wave approach as implemented in GPAW[60] in the framework of the Atomistic Simulation Environment (ASE).[61] The exchange-correlation interaction was treated by the generalized gradient approximation using the Perdew–Burke–Ernzerhof (PBE) functional.[62] The effect of the core electrons in the valence density was taken into account by means of the projector-augmented wave (PAW) method[63] with an energy cutoff of 450 eV. For some of the calculations, the on-site coulomb interactions of localized electrons were described by additionally adding a normalized effective Hubbard correction of U_{eff} = 4.1 eV, which results in a band gap of 3.065 eV. Optimized cell parameters of 3.810 Å and 9.760 Å have been calculated using a 11 × 11 × 11 k-point sampling of Monkhorst and Pack.[64] A 4 × 1 surface cell with four TiO_2 tri-layers was used for all calculations with ~12 Å vacuum to both sites of the slab. Due to the size of the repeating cell, a 3 × 3 × 1 k-point sampling of Monkhorst and Pack[64] was used. All atoms were allowed to fully

relax. The reaction and migration pathways were determined using the climbing-image elastic band method (ci-EB).[65]

Vibrational energies were calculated using finite difference in the harmonic approximation. Partial hessians considering just the adsorbed species (water or hydroxyls) were calculated, and the IR intensities were calculated from a finite difference approximation of the gradient of the dipole moment,[66] implemented in ASE.[61] The atomic mass of hydrogen was set to 2.014 g mol^{-1} in order to simulate vibrational spectra of deuterated species. For calculating the vibrational energies, the Hubbard correction was not used, because different U values tend to lead to larger variations of the vibrational energies.[67] In the ESI, we provide the Python script we used for simulating the IR spectra, which needs the calculated wavenumbers and intensities as input.

3 Results and discussion

H_2O exposure at room temperature. Fig. 1c shows an STM image of an a-TiO_2(101) surface that was exposed to 60 L H_2O at RT. The continuous rows of faint protrusions along the [010] direction originate from the 2f–O / 5f–Ti pairs of bare a-TiO_2(101),[31, 36] and the surface areas with brighter appearance (grayish) are associated with subsurface Ti*3d* electron donors.[32] The homogeneously distributed, bright protrusions (some marked by white circles in Fig. 1c) appeared after the water exposure. As will be shown below, these protrusions originate from pairs of terminal (OH_t) and bridging (OH_b) hydroxyl groups (see the computed structure in Fig. 1b). The rather low densities of OH_t / OH_b features found in this and additional RT experiments are plotted in Fig. S2 in the ESI. From now on we will denote a-TiO_2(101) surfaces with OH_t / OH_b–pairs as "a-TiO_2(101)–OH" (or "a-TiO_2(101)–OD", if D_2O was used for the hydroxylation).

The zoom-in STM image depicted in Fig. 1d we recorded within the same experiment as the STM image shown in Fig. 1c. However, a special tip state allowed us to resolve the OH_t / OH_b features with higher resolution, revealing dumbbell-like shapes and an apparent STM height of ~1 Å. The appearance and the STM height is similar to previously reported STM results of water molecules[33, 36, 44, 45, 53] and OH groups.[44, 53]

Although the observed STM features are similar to those of water molecules on a-TiO_2(101), such an assignment is inconsistent with other results: (i) Previous[35] and current TPD data (see Fig. S3 in the ESI) show that most of the first ML desorbs at temperatures clearly below RT. (ii) The diffusivity of water species on TiO_2 surfaces[36, 68] is rather high, so that STM imaging of them at RT is not possible with our instrument. Notice that the species observed here diffuse only very little at RT. Thus, it is unlikely that the observed features originate from water molecules.

Fig. 2a shows VB spectra of a-TiO_2(101) recorded before and after a high water exposure at RT (12 × 10^3 L). The most obvious difference in the VB spectra is the OH-*3σ* feature at a binding energy (BE) of ~11.0 eV that is evident in the spectrum of a-TiO_2(101)–OH. A faint OH-*1π* feature at ~8.0 eV BE can also be recognized in this VB spectrum, even though it is superimposed by the dominating O*2p* feature of TiO_2. For adsorbed water, three peaks are expected to appear within the VB (at ~8, ~11 and ~13 eV BE), whereas two peaks (at ~8 and ~11 eV BE), as found here, are characteristic for the presence of OH groups.[22, 38] It is evident that OH groups have formed at RT upon large water dose onto reduced a-TiO_2(101).

Ice-treatment. Motivated by previous studies[41, 44, 69] we altered the preparation of a-TiO_2(101)–OH such that more moderate water exposures were sufficient for the hydroxylation. More specifically, > ~5 ML water were dosed onto clean a-TiO_2(101) at low temperatures (< 140 K), followed by annealing at a temperature > ~180 K. Fig. 2b shows the VB spectrum acquired after applying this "ice-treatment" (green curve). Even though we used a much smaller water exposure (50 L at 130 K) compared to the RT experiment (12 × 10^3 L, see Fig. 2a), the degree of hydroxylation of the two compared a-TiO_2(101)–OH surfaces is similar. Fig. 2c depicts an STM image of an a-TiO_2(101)–OH surface that was obtained after applying the ice-treatment (likewise 50 L at 130 K). Again, we find the elongated protrusions originating from OH groups. The density of OH groups (~0.09 ML) was four to five times higher than in the experiment corresponding to Fig. 1c,d (~0.02 ML), where the water exposure was similar but accomplished at RT. Accordingly, a-TiO_2(101)–OH surfaces with rather high OH densities can be created when applying the ice-treatment. In addition to our STM and VB studies, we conducted TPD experiments addressing the ice-treatment (see Fig. S4 in the ESI).

To disclose the nature of the hydroxyl groups on a-TiO_2(101)–OH, we conducted IRRAS experiments. In the IRRAS experiments, we worked preferentially with D_2O to avoid interference with residual H_2O in the UHV chamber. Here we focus on IRRAS data obtained for p-polarized light, thus we are probing vibrations with transition dipole moments

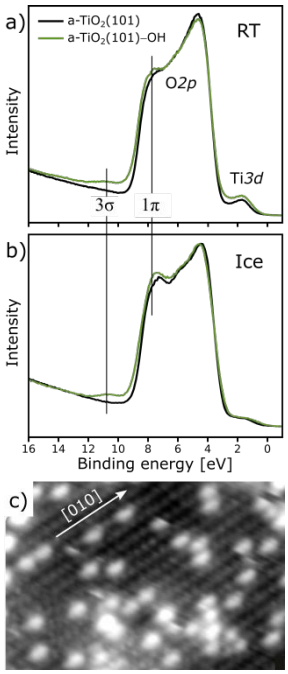

Fig. 2 Two preparation methods for a-TiO_2(101)–OH. (a) VB spectra of a-TiO_2(101) before and after 12× 10^3 L H_2O exposure at RT (black and green curves, respectively). The spectra were recorded at RT. (b) VB spectrum of bare a-TiO_2(101) (black curve) and after applying the ice-treatment (50 L H_2O exposure at 130 K, followed by annealing at RT) (green curve). The spectra were recorded at 600 K (black curve) and RT (green curve). (c) STM image (15 × 10 nm; RT) of a-TiO_2(101)–OH acquired after 50 L H_2O exposure at 130 K and subsequent annealing at RT.

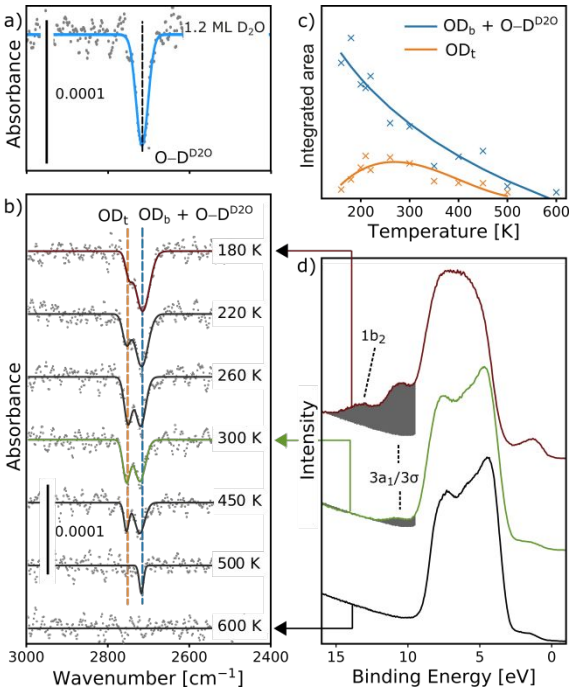

Fig. 3 IRRAS and VB measurements upon applying the ice-treatment. (a) IRRAS spectrum (p-polarized light) of D_2O / a-TiO_2(101) at 30 K. 1 ML D_2O was dosed at 120 K. Data points shown in gray. A single peak at ~2715 cm^{-1} is seen (curve fit in blue). (b) Selected IRRAS spectra of the O–D stretch, measured at 30 K, obtained after 5 ML D_2O exposure onto clean a-TiO_2(101) followed by annealing for 600 s at the given temperatures. Two peaks are resolved: One centered at ~2715 cm^{-1} (blue dashed line) and one at ~2751 cm^{-1} (orange dashed line). Curve fits are shown in maroon (annealing at 180 K), green (annealing at 300 K), and black (annealing at 220, 260, 450, 500 and 600 K). (c) Integrated areas (from the 2-peak curve fitting) of the peaks at ~2715 cm^{-1} (blue data points) and ~2751 cm^{-1} (orange data points) as function of annealing temperature. Solid lines in blue and orange guide the eye. Notice that the number of data points in c) is higher than the number of spectra in b) because only selected spectra are shown. (d) VB spectra acquired after exposing a clean a-TiO_2(101) surface to 50 L H_2O at 130 K followed by annealing for 600 s at the specified temperatures (180 K: maroon curve; 300 K: green curve; 600 K: black curve). VB data acquisition was accomplished at the given annealing temperatures. Gray areas show the differences to the VB spectrum of clean TiO_2 (black curve) for 9 eV ≤ BE ≤ 16.5 eV.

perpendicular to the (101) surface and also parallel to the surface in the direction of the IR beam (see Fig. S1). For reference, Fig. 3a shows an IRRAS spectrum of 1.2 ML molecular water (D_2O) adsorbed on the a-TiO_2(101) surface. This spectrum was recorded at 30 K, after a D_2O exposure at 120 K. The single peak centered at ~2715 cm^{-1} originates from O–D stretching vibrations in water molecules (denoted O–D^{D2O}). IRRAS spectra obtained with s-polarized light do not show any appreciable peaks exceeding noise (see Fig. S5 in the ESI).

Fig. 3b shows IRRAS spectra acquired upon applying the ice-treatment. That is, we exposed an a-TiO_2(101) surface to 6 ML D_2O, followed by annealing at specified temperatures, in each case for 600 s. Each spectrum was acquired after starting with a clean a-TiO_2(101) surface. Following annealing at the selected temperatures, we found two peaks in the IRRAS spectra: (i) one at ~2715 cm^{-1} (blue dashed line) and, (ii), one at ~2751 cm^{-1} (orange dashed line). These peaks partly overlap each other. As argued in the following, the first peak can originate both from the O–D stretch of molecular water (O–D^{D2O}), see Fig. 3a, *and* the O–D stretch of bridging hydroxyls (OD_b). From now on, we refer to this peak as "O–D^{D2O} + OD_b peak". The second peak at ~2751 cm^{-1} we assign below to terminal hydroxyls (OD_t), and is from now on denoted as "OD_t peak".

Following annealing at 180 K, the OD_t peak (orange dashed line) appeared as a shoulder of the O–D^{D2O} + OD_b peak, see Fig. 3b. As seen in Fig. 3b,c, the OD_t peak was most intense following annealing between 200 and 300 K and was diminished for annealing temperatures above 450 K. There was no shift of the OD_t peak throughout the series of IRRAS spectra. In contrast, the O–D^{D2O} + OD_b peak was detected in all IRRAS spectra up to annealing at 450 K, see Fig. 3b. Only annealing at temperatures higher than 500 K led to the disappearance of this peak. The O–D^{D2O} + OD_b peak was most intense at low annealing temperatures, and its intensity decreased continuously with increasing annealing temperature, see Fig. 3c. In addition, the O–D^{D2O} + OD_b peak blue-shifted slightly (by ~5 cm^{-1}) upon annealing at temperatures higher than 220 K.

To facilitate a direct comparison of the IRRAS data with our VB data, we show (again) VB data in Fig. 3d. The VB spectra in Fig. 3d were acquired following a 50 L H_2O exposure at 130 K and subsequent annealing at either 180 K (maroon curve), 300 K (green curve) or 600 K (black curve). Considering the uppermost IRRAS spectrum in Fig. 3b and the uppermost VB spectrum in Fig. 3d (maroon curves), we find that annealing at 180 K led to a-TiO_2(101) surfaces that were covered with water molecules (in the sub-ML range). Otherwise, there should not be any states at ~13 eV BE in the blue VB spectrum that originate from $1b_2$ water orbitals. In addition, the broad peak centered at ~11 eV BE indicates a dominating contribution of the $3a_1$ state of molecularly adsorbed water. Accordingly, the O–D^{D2O} + OD_b peak in the uppermost IRRAS spectrum of Fig. 3b originates largely from molecularly adsorbed water.

The situation is different when the annealing temperature was 300 K (see the green curves in Fig. 3b,d). In the VB spectrum, there is only a feature of low intensity at ~11 eV BE and no peak at ~13 eV BE (Fig. 3d). As already argued in connection with Fig. 2b, this VB spectrum indicates the presence of OH groups and the absence of molecular water. That there is barely any molecularly water adsorbed on the surface after annealing at 300 K is further supported by ESD measurements presented in the ESI, see Fig. S6–S8. Nevertheless, there is a peak at ~2715 cm^{-1} in the corresponding IRRAS data (green spectrum in Fig. 3b). Accordingly, the O–D^{D2O} + OD_b peaks in the IRRAS data of Fig. 3b did not originate from molecularly adsorbed water when the annealing temperature was ~RT or higher. Taking the IRRAS and VB data together, we conclude that both, molecular water *and* hydroxyls, contribute to the IRRAS peak at ~2715 cm^{-1}. The IRRAS spectrum obtained following annealing at 180 K (maroon curve in Fig. 3b) is composed of three peaks: Two belonging to hydroxyl groups (positioned at ~2751 cm^{-1} and ~2715 cm^{-1}) and one belonging to molecular water, likewise positioned at ~2715 cm^{-1}.

Isotope-labeling experiments. To ascertain the assignments of the hydroxyl-related peaks in the IRRAS spectra we performed isotope-labeling experiments, using $H_2{}^{16}O$ and $H_2{}^{18}O$ (see Fig. 4). Thus, we

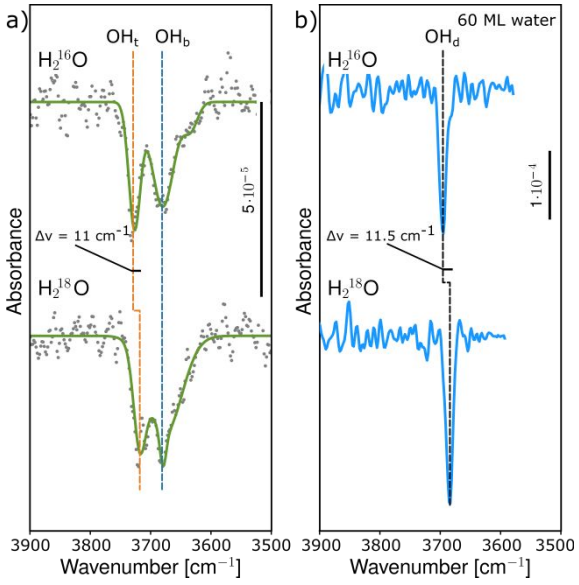

Fig. 4 Isotope-labeling IRRAS experiments on a-TiO_2(101)–OH. (a) IRRAS spectrum of the O–H stretch, measured at 30 K, obtained after 6 ML water exposures at 120 K followed by annealing at 350 K for 600 s. Both, $H_2{}^{16}O$ (upper spectrum) and $H_2{}^{18}O$ (lower spectrum) isotopes were used to prepare the a-TiO_2(101)–OH surfaces. The peak on the left at the higher frequency red-shifts by ~11 cm^{-1} (orange dashed line). The peak on the right (blue dashed line) does not depend on the oxygen isotope. (b) Internal reference of the shift observed in a). 60 ML of $H_2{}^{16}O$ (upper spectrum) and 60 ML of $H_2{}^{18}O$ (lower spectrum) were dosed at 120 K to prepare thick water ice layers. Data acquisition at 30 K. The measured region includes the dangling O–H stretches (baseline subtracted).

inspected the O–H stretch rather than the O–D stretch. The results allow us to clearly distinguish between OH_t and OH_b groups in the IRRAS spectra. Exchanging ^{16}O with ^{18}O within the water adsorbate should exclusively lead to a shift of the OH_t–related peak. The OH_b–related peak in the IRRAS spectra is not expected to shift because the O's of OH_b species belong to the a-TiO_2(101) surface (see Fig. 1b). Fig. 4a shows IRRAS spectra acquired after exposures of $H_2{}^{16}O$ (upper spectrum) and $H_2{}^{18}O$ (lower spectrum) followed by annealing at 350 K for 600 s. In each case, the water exposure was 6 ML and the sample temperature upon adsorption was 120 K. Such sample preparations result in a-TiO_2(101)–OH surfaces without residual adsorbed molecular water. Within the OH–related doublet, exclusively the left peak at higher frequency ($^{16}OH_t$: ~3729 cm^{-1} for $H_2{}^{16}O$ and $^{18}OH_t$: ~3718 cm^{-1} for $H_2{}^{18}O$) shifted upon the change of the water isotope (see Fig. 4a). Specifically, we observed a red shift by ~11 cm^{-1} of the left peak whereas the right peak did not shift ($^{16}OH_b$: ~3681 cm^{-1} for both $H_2{}^{16}O$ and $H_2{}^{18}O$). Assuming a harmonic potential in the time dependent Schrödinger equation, we estimated a red shift of the OH_t–related IRRAS peak by ~12 cm^{-1} if ^{16}O is replaced by ^{18}O.

As an internal reference, we have also measured the O–H stretch of dangling hydroxyls (non-hydrogen bonded water molecules), OH_d, of a thick ice layer adsorbed on a-TiO_2(101), see Fig. 4b. In each case, the water exposure ($H_2{}^{18}O$ and $H_2{}^{16}O$, respectively) at 120 K was 60 ML. We observed a red shift of the O–H stretch by ~11.5 cm^{-1} when $H_2{}^{18}O$ was used instead of $H_2{}^{16}O$. This red shift is very close to the expected shift of ~12 cm^{-1}.

From the isotope-labeling experiments, we can conclude with certainty that the left IRRAS peak of the hydroxyl doublet at the higher frequency originates from OH_t and OD_t, respectively, and the peak on the right (at lower frequency) from bridging hydroxyls, OH_b or OD_b. With regard to Fig. 3b, it is clear that the peak at ~2751 cm^{-1} originates from OD_t. The peak at ~2715 cm^{-1} can originate from molecular D_2O (no annealing), from deuterium atoms adsorbed on 2f–O surface sites (i.e. from OD_b), or from a mixture of molecular D_2O and OD_b species. The position of OD_b found here is very close to the earlier reported OD_b–IRRAS peak (at 2721 cm^{-1}) obtained following dissociation of D_2O molecules at bridging O_{vac}'s that were created via electron bombardment.[48]

With these assignments of the IRRAS peaks, we can explain the observed trends of the integrated peak areas as a function of the annealing temperature seen in Fig. 3c. Without any annealing of the sample, the $O–D^{D2O}$ + OD_b peak is large because the a-TiO_2(101) surface was covered by molecularly adsorbed water. Upon subsequent annealing at temperatures > 140 K, a part of the adsorbed water molecules desorbed from the sample (see Refs. [35, 48] and Fig. S4 in the ESI). Upon annealing at 160–300 K, further water desorbed and some water molecules dissociated, leading to OD_t / OD_b–pairs on the surface. The latter leads to the OD_t peak in the IRRAS spectra. The integrated area of the $O–D^{D2O}$ + OD_b peak does not clearly decline upon water dissociation because the OD_b hydroxyls also contribute to this peak. The small blue shift of the $O–D^{D2O}$ + OD_b peak by ~5 cm^{-1} upon annealing at temperatures higher than 220 K is probably associated with the change of the adsorbate from D_2O to OD_b.

The peak assignments put forward here likewise agree well with very early studies addressing TiO_2 nanoparticles that indicated OH_t groups to vibrate at higher frequencies than OH_b groups.[70, 71] Whereas OH–related features observed on TiO_2 nanoparticles at frequencies higher than 3700 cm^{-1} are mostly assigned to OH_t groups, vibrational bands at lower frequencies are often assigned to OH_b groups.[72, 73]

DFT calculations. To understand the mechanism for water dissociation on reduced a-TiO_2(101), we have performed a set of DFT calculations. We used mainly plain DFT with the PBE functional, but also addressed spurious electron delocalization using Hubbard-U corrections. Most DFT+U energies are close to those computed with plain PBE-DFT (see Table 1). In the following text, we only refer to the results obtained with plain DFT.

Using a slab of stoichiometric a-TiO_2(101) – labeled sa-TiO_2 in Table 1 and Fig. 5, we found that the most stable structure of molecular water (see Fig. 1a und 5a) is favored over dissociated water (see Fig. 1b und 5b) by ~0.32 eV. This result is in good agreement with previous results.[33, 36, 50] However, when the a-TiO_2(101) slab is reduced via removal of one O atom (i.e. through the introduction of an O_{vac}; labeled ra-TiO_2 in Table 1 and Fig. 5), dissociative adsorption of water is more favorable than molecular adsorption. Fig. 5c shows the calculated PBE energies for three different positions of the O_{vac} that are labeled "position 1", "position 2" and "position 3". For example, the OH_t / OH_b–pair configuration is favored by ~0.15 eV if the O_{vac} is placed between the first and second TiO_2 tri-layer beneath of the adsorbate (position 1). In addition, we found that the barrier

Table 1 Relative adsorption energies (in eV) of the considered H_2O and hydroxyl structures on ra-TiO_2 and sa-TiO_2 slabs computed with PBE and PBE+U. Minus signs indicate that the hydroxyl structures are more stable than molecular water. For the O_{vac} positions, see Fig. 5.

ra-TiO_2	PBE	PBE+U
O_{vac} at position 1: molecular water on 5f–Ti *vs*. OH_t / OH_b	–0.15	–0.11
O_{vac} at position 2: molecular water on 5f–Ti *vs*. OH_t / OH_b	–0.16	–0.05
O_{vac} at position 3: molecular water on 5f–Ti *vs*. OH_t / OH_b	–0.35	–0.20
O_{vac} at position 3: molecular water on 5f–Ti *vs*. 2 × OH_b	–0.42	–0.62
O_{vac} at position 3: molecular water in O_{vac} *vs*. 2 × OH_b	–0.59	–0.58
sa-TiO_2(101)		
no O_{vac}: molecular water on 5f–Ti *vs*. OH_t / OH_b	+0.32	+0.29

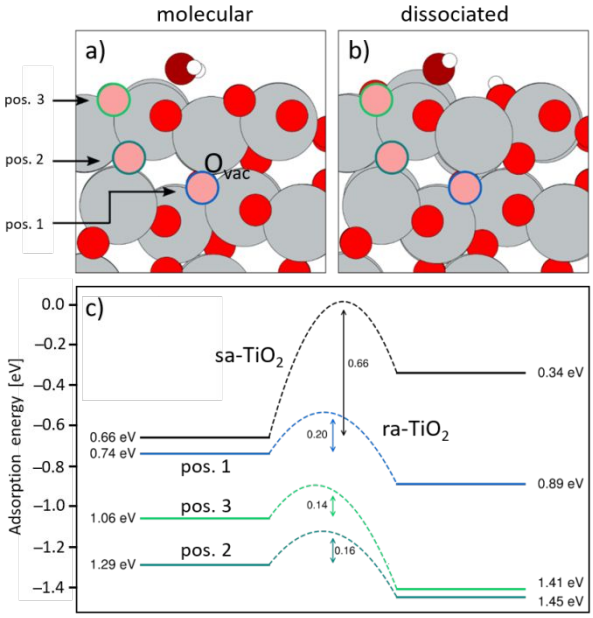

Fig. 5 Water adsorption structures found by DFT calculations (PBE), showing that OH_t / OH_b–pairs are on reduced a-TiO_2(101) more stable than water molecules. (a) Ball model (side view) of molecularly adsorbed water on a-TiO_2(101) (color-coding as in Fig. 1). The lowest energy structure is shown that was found for a stoichiometric a-TiO_2(101) slab (sa-TiO_2). Considered positions of an O_{vac} within an reduced a-TiO_2(101) slab (ra-TiO_2) are also indicated. The corresponding top view is shown in Fig. 1a. (b) Ball model of an OH_t / OH_b–pair on ra-TiO_2 (side view). The lowest energy structure is shown that was found with the O_{vac} at position 1 (see corresponding top view in Fig. 1b). (c) Computed adsorption energies of molecularly adsorbed water (on the left) and of an OH_t / OH_b–pair on a-TiO_2(101) (on the right). Computed dissociation barriers are also given (middle). See also Fig. S11 in the ESI.

for water dissociation is low regardless of the exact position of the O_{vac} within the slab. Water dissociation is favorable for all considered ra-TiO_2 slabs (see Table 1 and Fig. S11 in the ESI). Notice that also an OH_t / OH_b–pair next to a surface O_{vac} is more stable than molecular water on 5f–Ti. Thus, "healing" of the surface O_{vac} is not an essential reaction step for water dissociation.

However, an OH_t / OH_b–pair is not the most-stable configuration of adsorbed water. Instead, a configuration consisting of two OH_b species (see Fig. S9 and S11) is more stable by ~0.42 eV compared to molecular water on a 5f–Ti site. Such a "2 × OH_b configuration" results if the subsurface O_{vac} in the considered ra-TiO_2 slab can diffuse to the surface, where it is filled by the OH_t group. When considering an ra-TiO_2 slab with one O_{vac}, this scenario is characterized by very low barriers, in agreement with Ref. [51]. Notice that the considered ra-TiO_2 slab is modeling only initially a bulk-reduced a-TiO_2(101) sample because the O_{vac} is "healed" upon reaction with the water molecule and 2 × OH_b configurations are located on the very surface.

To better model the diffusion of O_{vac}'s in bulk-reduced a-TiO_2(101), we also considered ra-TiO_2(101) slabs with more excess electrons. Specifically, we used plain DFT and a 3 × 3 × 1 bulk supercell. Depending on the O_{vac} concentration, we found O_{vac} diffusion barriers between 0.1 and 0.2 eV. This is similar as found for the ra-TiO_2 surface slab considered above. However, the diffusion barrier increased dramatically to ~0.95 eV after adding two additional excess electrons to the supercell. The computed O_{vac} diffusion barriers are almost independent on the O_{vac} concentration. Instead, the O_{vac} diffusion barriers correlate with the number of excess electrons within the supercell. Such high O_{vac} diffusion barriers agree well with previously published data.[34] Accordingly, the water dissociation mechanism proposed by Li and Gao[51] does not operate on bulk-reduced a-TiO_2(101) samples at low temperatures. If O_{vac}'s cannot diffuse to the surface, water dissociation leads to the formation of OH_t / OH_b–pairs, as observed experimentally. However, if O_{vac}'s can diffuse to the surface and water is present, a-TiO_2(101) with OH_b groups and without OH_t species are expected.

Finally, we have simulated IRRAS spectra corresponding to the found adsorbate structures (see Fig. S9 and Table S1 in the ESI). Although there is a constant shift of the modeled IRRAS peaks with respect to the experimentally found peak positions (because of the PBE functional), all essential features are reproduced. The peak corresponding to OD_t lays ~50 cm^{-1} higher than that of the OD_b, and the antisymmetric stretching vibration of water and the stretching vibration of OD_b differ only by a few wavenumbers, thus are almost degenerated, as experimentally observed. These results are strong support for the described IRRAS peak assignments, and thus confirm that pairs of terminal and bridging hydroxyls have formed.

The formation of thermally stable and well-separated OH_t / OH_b–pairs on otherwise bare a-TiO_2(101) surfaces is not possible on stoichiometric a-TiO_2(101). Previously, a fraction of dissociated water species has been predicted for full water ML's on stoichiometric a-TiO_2(101), i.e. when the OH groups, resulting from water dissociation events, are surrounded by non-dissociated water molecules.[52] Here, we do not have such a surrounding of water adsorbates, at least not in experiments conducted at RT and for T_{ann} ≥ 350 K. We thus consider the presented data as strong evidence for the influence of subsurface defects on the adsorption of water on

reduced a-TiO_2(101), in agreement with previous results.[33, 37] An important unresolved question is how the level of bulk reduction for the a-TiO_2(101) samples influences the extent of dissociative adsorption on the (101) surface. Our preliminary IRRAS data taken on a less reduced sample show relatively lower amounts of hydroxyls species.

The described dissociation mechanism for water / a-TiO_2(101) differs significantly from that one known for water / r-TiO_2(110), where water molecules dissociate directly at surface O_{vac}'s.[9, 14, 15, 18-24] Because any strong geometric contribution in favor of water dissociation such as "filling of O_{vac}'s" can be ruled out, we can conclude that predominantly electronic effects cause water dissociation events on a-TiO_2(101). Our data also reveal that the adsorption temperature plays an important role. Adsorption experiments conducted at low temperatures (< 200 K) point to molecular adsorption of water.[36] This is plausible considering that, (i), the water coverage was low in these experiments and, (ii), subsurface O_{vac}'s are immobile at such temperatures.[74] However, for temperatures > 200 K, where subsurface O_{vac}'s are eventually mobile,[74] combined with sufficiently large water exposures, the influence of subsurface O_{vac}'s is high enough to measure that molecular water adsorption is not the only adsorption mode. These differences explain why most XPS studies pointed toward mixed dissociative / molecular water adsorption, whereas most previous STM studies concluded molecular adsorption of water on a-TiO_2(101).

4 Conclusions

In this combined experimental and theoretical work, we have obtained atomic-scale insight into a very fundamental problem –the dissociation of water molecules on bulk-reduced anatase TiO_2(101). We reached the following conclusions: (i) As the result of water dissociation, pairs of terminal and bridging hydroxyls (OH_t / OH_b– or OD_t / OD_b–pairs) form on the surface. Both, large water exposures at RT and the ice-treatment (annealing of water multilayers) lead to the formation of such hydroxyl pairs. (ii) Both, molecular water and bridging hydroxyl groups exhibit quite similar IRRAS peaks at ~2715 cm^{-1} (for D_2O). OD_t groups are characterized by a peak at ~2751 cm^{-1} and thus their signature in IRRAS is blue shifted by ~35 cm^{-1} compared to that of OD_b groups. (iii) The hydroxyl pairs are thermally quite stable species on the a-TiO_2(101) surface. Annealing at temperatures higher than 500 K is required to completely remove the hydroxyl pairs. (iv) On the basis of DFT calculations, we found that the dissociation of water molecules on a-TiO_2(101) is driven by O_{vac}'s in the subsurface region, and there is no need for O_{vac}'s to diffuse to the surface to make water dissociation possible. (v) The diffusion of O_{vac}'s in the bulk of a-TiO_2 is strongly influenced by the degree of a-TiO_2 reduction. The more excess electrons are present in the bulk, the higher are the O diffusion barriers.

Author contributions

K.C.A., N.G.P., W.D., G.A.K., B.H., J.V.L., and S.W. designed research; K.C.A., N.G.P., W.D., T.X., L.L. and Z.L. performed research; K.C.A., and N.G.P. analyzed data; S.W., K.C.A, W.D., and N.G.P. wrote the paper.

Conflicts of interest

There are no conflicts to declare.

Acknowledgements

We acknowledge support from the Innovation Fund Denmark (IFD), File No. 6151-00008B (ProNOx), the Villum Fonden (Investigator grant, Project No. 16562), the Danish National Research Foundation through the Center of Excellence "InterCat" (Grant agreement no: DNRF150), and Haldor Topsoe A/S. We acknowledge beam time received at ASTRID2 on the MATLine beamline. This work was also supported by the US Department of Energy, Office of Science, Office of Basic Energy Sciences, Division of Chemical Sciences, Geosciences, & Biosciences and performed in EMSL, a national scientific user facility sponsored by the Department of Energy's Office of Biological and Environmental Research and located at Pacific Northwest National Laboratory (PNNL). PNNL is a multiprogram national laboratory operated for DOE by Battelle. We acknowledge financial support through the APF project 'Materials on Demand' within the 'Humans on Mars' Initiative funded by the Federal State of Bremen and the University of Bremen.

Notes and references

1 S. J. Tauster, *Accounts Chem. Res.* 1987, **20**, 389–394.
2 G. Busca, L. Lietti, G. Ramis and F. Berti, *Appl. Catal. B-Environ.* 1998, **18**, 1–36.
3 G. E. Brown, V. E. Henrich, W. H. Casey, D. L. Clark, C. Eggleston, A. Felmy, D. W. Goodman, M. Gratzel, G. Maciel, M. I. McCarthy, K. H. Nealson, D. A. Sverjensky, M. F. Toney and J. M. Zachara, *Chem. Rev.* 1999, **99**, 77–174.
4 M. Grätzel, *Nature* 2001, **414**, 338–344.
5 A. Gurlo and R. Riedel, *Angew. Chem.-Int. Edit.* 2007, **46**, 3826–3848.
6 X. Chen and S. S. Mao, *Chem. Rev.* 2007, **107**, 2891–2959.
7 U. Diebold, *Surf. Sci. Rep.* 2003, **48**, 53–229.
8 A. Fujishima, X. Zhang and D. A. Tryk, *Surf. Sci. Rep.* 2008, **63**, 515–582.
9 M. A. Henderson, *Surf. Sci. Rep.* 2011, **66**, 185–297.
10 M. Kapilashrami, Y. F. Zhang, Y. S. Liu, A. Hagfeldt and J. H. Guo, *Chem. Rev.* 2014, **114**, 9662–9707.
11 M. A. Henderson, *Surf. Sci. Rep.* 2002, **46**, 5–308.
12 E. Bjornehohn, M. H. Hansen, A. Hodgson, L. M. Liu, D. T. Limmer, A. Michaelides, P. Pedevilla, J. Rossmeisl, H. Shen, G. Tocci, E. Tyrode, M. M. Walz, J. Werner and H. Bluhm, *Chem. Rev.* 2016, **116**, 7698–7726.
13 R. T. Mu, Z. J. Zhao, Z. Dohnálek, J. L. Gong, *Chem. Soc. Rev.* 2017, **46**, 1785–1806.

14 Z. Dohnálek, I. Lyubinetsky and R. Rousseau, *Prog. Surf. Sci.* 2010, **85**, 161–205.
15 C. L. Pang, R. Lindsay, G. Thornton, *Chem. Rev.* 2013, **113**, 3887–3948.
16 M. Setvin, M. Wagner, M. Schmid, G. S. Parkinson, U. Diebold, *Chem. Soc. Rev.* 2017, **46**, 1772–1784.
17 L. X. Wu, C. Fu and W. X. Huang, *Phys. Chem. Chem. Phys.* 2020, **22**, 9875–9909.
18 B. Hammer, S. Wendt and F. Besenbacher, *Top. Catal.* 2010, **53**, 423–430.
19 S. Wendt, R. Schaub, J. Matthiesen, E. K. Vestergaard, E. Wahlström, M. D. Rasmussen, P. Thostrup, L. M. Molina, E. Lægsgaard, I. Stensgaard, B. Hammer and F. Besenbacher, *Surf. Sci.* 2005, **598**, 226–245.
20 S. Wendt, J. Matthiesen, R. Schaub, E. K. Vestergaard, E. Lægsgaard, F. Besenbacher and B. Hammer, *Phys. Rev. Lett.* 2006, **96**, 066107.
21 H. H. Kristoffersen, J. Ø. Hansen, U. Martinez, Y. Y. Wei, J. Matthiesen, R. Streber, R. Bechstein, E. Lægsgaard, F. Besenbacher, B. Hammer and S. Wendt, *Phys. Rev. Lett.* 2013, **110**, 146101.
22 R. L. Kurtz, R. Stockbauer, T. E. Madey, E. Román and J. L. de Segovia, *Surf. Sci.* 1989, **218**, 178–200.
23 M. B. Hugenschmidt, L. Gamble, C. T. Campbell, *Surf. Sci.* 1994, **302**, 329–340.
24 M. A. Henderson, *Surf. Sci.* 1996, **355**, 151–166.
25 G. Ketteler, S. Yamamoto, H. Bluhm, K. Andersson, D. E. Starr, D. F. Ogletree, H. Ogasawara, A. Nilsson and M. Salmeron, *J. Phys. Chem. C* 2007, **111**, 8278–8282.
26 S. J. Tan, H. Feng, Y. F. Ji, Y. Wang, J. Zhao, A. D. Zhao, B. Wang, Y. Luo, J. L. Yang and J. G. Hou, *J. Am. Chem. Soc.* 2012, **134**, 9978–9985.
27 Z. T. Wang, Y. G. Wang, R. Mu, Y. H. Yoon, A. Dahal, G. K. Schenter, V. A. Glezakou, R. Rousseau, I. Lyubinetsky and Z. Dohnálek, *Proc. Natl. Acad. Sci. U. S. A.* 2017, **114**, 1801–1805.
28 U. Diebold, *J. Chem. Phys.* 2017, **147**, 3.
29 T. Ohno, K. Sarukawa, K. Tokieda and M. Matsumura, *J. Catal.* 2001, **203**, 82–86.
30 M. Setvin, B. Daniel, V. Mansfeldova, L. Kavan, P. Scheiber, M. Fidler, M. Schmid and U. Diebold, *Surf. Sci.* 2014, **626**, 61–67.
31 S. Koust, L. Arnarson, P. G. Moses, Z. S. Li, I. Beinik, J. V. Lauritsen and S. Wendt, *Phys. Chem. Chem. Phys.* 2017, **19**, 9424–9431.
32 Y. B. He, O. Dulub, H. Z. Cheng, A. Selloni and U. Diebold, *Phys. Rev. Lett.* 2009, **102**, 106105.
33 U. Aschauer, Y. B. He, H. Z. Cheng, S. C. Li, U. Diebold and A. Selloni, *J. Phys. Chem. C* 2010, **114**, 1278–1284.
34 P. Scheiber, M. Fidler, O. Dulub, M. Schmid, U. Diebold, W. Y. Hou, U. Aschauer and A. Selloni, *Phys. Rev. Lett.* 2012, **109**, 136103.
35 G. S. Herman, Z. Dohnálek, N. Ruzycki, U. Diebold, *J. Phys. Chem. B* 2003, **107**, 2788–2795.
36 Y. B. He, A. Tilocca, O. Dulub, A. Selloni and U. Diebold, *Nat. Mater.* 2009, **8**, 585–589.
37 M. J. Jackman, A. G. Thomas and C. Muryn, *J. Phys. Chem. C* 2015, **119**, 13682–13690.
38 D. T. Payne, Y. Zhang, C. L. Pang, H. H. Fielding and G. Thornton, *Top. Catal.* 2017, **60**, 392–400.
39 I. M. Nadeem, G. T. Harrison, A. Wilson, C. L. Pang, J. Zegenhagen and G. Thornton, *J. Phys. Chem. B* 2018, **122**, 834–839.
40 I. M. Nadeem, J. P. W. Treacy, S. Selcuk, X. Torrelles, H. Hussain, A. Wilson, D. C. Grinter, G. Cabailh, O. Bikondoa, C. Nicklin, A. Selloni, J. Zegenhagen, R. Lindsay and G. Thornton, *J. Phys. Chem. Lett.* 2018, **9**, 3131–3136.
41 L. E. Walle, A. Borg, E. M. J. Johansson, S. Plogmaker, H. Rensmo, P. Uvdal and A. Sandell, *J. Phys. Chem. C* 2011, **115**, 9545–9550.
42 A. Schaefer, V. Lanzilotto, U. B. Cappel, P. Uvdal, A. Borg and A. Sandell, *Langmuir* 2018, **34**, 10856–10864.
43 A. Schaefer, V. Lanzilotto, U. Cappel, P. Uvdal, A. Borg and A. Sandell, *Surf. Sci.* 2018, **674**, 25–31.
44 C. Dette, M. A. Perez-Osorio, S. Mangel, F. Giustino, S. J. Jung, K. Kern, *J. Phys. Chem. C* 2017, **121**, 1182–1187.
45 M. Setvin, B. Daniel, U. Aschauer, W. Hou, Y. F. Li, M. Schmid, A. Selloni and U. Diebold, *Phys. Chem. Chem. Phys.* 2014, **16**, 21524–21530.
46 C. Dette, M. A. Perez-Osorio, S. Mangel, F. Giustino, S. J. Jung, K. Kern, *J. Phys. Chem. C* 2018, **122**, 11954–11960.
47 A. Dahal and Z. Dohnálek, *J. Phys. Chem. C* 2017, **121**, 20413–20418.
48 N. A. Deskins, G. A. Kimmel and N. G. Petrik, *J. Phys. Chem. Lett.* 2020, **11**, 9289–9297.
49 A. Vittadini, A. Selloni, F. P. Rotzinger and M. Grätzel, *Phys. Rev. Lett.* 1998, **81**, 2954–2957.
50 A. Tilocca and A. Selloni, *J. Phys. Chem. B* 2004, **108**, 4743–4751.
51 Y. D. Li and Y. Gao, *Phys. Rev. Lett.* 2014, **112**, 206101.
52 C. E. Patrick and F. Giustino, *Phys. Rev. Appl.* 2014, **2**, 014001.
53 M. Setvin, U. Aschauer, J. Hulva, T. Simschitz, B. Daniel, M. Schmid, A. Selloni and U. Diebold, *J. Am. Chem. Soc.* 2016, **138**, 9565–9571.
54 G. Fisicaro, S. Filice, S. Scalese, G. Compagnini, R. Reitano, L. Genovese, S. Goedecker, I. Deretzis and A. La Magna, *J. Phys. Chem. C* 2020, **124**, 2406–2419.
55 E. Lægsgaard, F. Besenbacher, K. Mortensen, I. Stensgaard, *J. Microsc.* 1988, **152**, 663–669.
56 J. V. Lauritsen, F. Besenbacher, *Adv. Catal.* 2006, **50**, 97–147.
57 Y. J. Li, K. C. Adamsen, L. Lammich, J. V. Lauritsen and S. Wendt, *ACS Nano* 2019, **13**, 11632–11641.
58 Z. Li, https://www.isa.au.dk/facilities/astrid2/beamlines/AU-Matline/AU-Matline.asp.
59 A. Dahal, N. G. Petrik, Y. Q. Wu, G. A. Kimmel, F. Gao, Y. Wang and Z. Dohnálek, J. Phys. Chem. C 2019, **123**, 24133–24145.
60 J. Enkovaara, C. Rostgaard, J. J. Mortensen, J. Chen, M. Dułak, L. Ferrighi, J. Gavnholt, C. Glinsvad, V. Haikola, H. A. Hansen, H. H. Kristoffersen, M. Kuisma, A. H. Larsen, L. Lehtovaara, M. Ljungberg, O. Lopez-Acevedo, P. G. Moses, J. Ojanen, T. Olsen, V. Petzold, N. A. Romero, J. Stausholm-Møller, M. Strange, G. A. Tritsaris, M. Vanin, M. Walter, B. Hammer, H. Häkkinen, G. K. H. Madsen, R. M. Nieminen, J. K. Nørskov, M. Puska, T. T. Rantala, J. Schiøtz, K. S. Thygesen and K. W. Jacobsen, *J. Phys.-Condes. Matter* 2010, **22**, 253202.
61 A. H. Larsen, J. J. Mortensen, J. Blomqvist, I. E. Castelli, R. Christensen, M. Dulak, J. Friis, M. N. Groves, B. Hammer, C. Hargus, E. D. Hermes, P. C. Jennings, P. B. Jensen, J. Kermode, J. R. Kitchin, E. L. Kolsbjerg, J. Kubal, K. Kaasbjerg, S. Lysgaard, J. B. Maronsson, T. Maxson, T. Olsen, L. Pastewka, A. Peterson, C. Rostgaard, J. Schiotz, O. Schutt, M. Strange, K. S. Thygesen, T. Vegge, L. Vilhelmsen, M. Walter, Z. H. Zeng and K. W. Jacobsen, *J. Phys.-Condes. Matter* 2017, **29**, 30.
62 J. P. Perdew, K. Burke and M. Ernzerhof, *Phys. Rev. Lett.* 1996, **77**, 3865–3868.
63 P. E. Blöchl, *Phys. Rev. B* 1994, **50**, 17953–17979.
64 H. J. Monkhorst and J. D. Pack, *Phys. Rev. B* 1976, **13**, 5188–5192.
65 E. L. Kolsbjerg, M. N. Groves and B. Hammer, *J. Chem. Phys.* 2016, **145**, 9.

66 D. Porezag and M. R. Pederson, *Phys. Rev. B* 1996, **54**, 7830–7836.
67 E. German, R. Faccio and A. W. Mombru, *J. Phys. Commun.* 2017, **1**, 10.
68 J. Matthiesen, J. Ø. Hansen, S. Wendt, E. Lira, R. Schaub, E. Lægsgaard, F. Besenbacher and B. Hammer, *Phys. Rev. Lett.* 2009, **102**, 226101.
69 S. Koust, K. C. Adamsen, T. Xu, I. Beinik, Z. S. Li, J. V. Lauritsen and S. Wendt, *J. Phys. Chem. C* 2020, **124**, 26916–26924.
70. M. Primet, P. Pichat and M. V. Mathieu, *J. Phys. Chem.* 1971, **75**, 1216–1220.
71 A. A. Tsyganenko and V. N. Filimonov, *J. Mol. Struct.* 1973, **19**, 579–589.
72 C. Deiana, E. Fois, S. Coluccia and G. Martra, *J. Phys. Chem. C* 2010, **114**, 21531–21538.
73 L. Mino, A. Morales-Garcia, S. T. Bromley and F. Illas, *Nanoscale* 2021, **13**, 6577–6585.
74 M. Setvin, M. Schmid and U. Diebold, *Phys. Rev. B* 2015, **91**, 195403.